Wavelet-Feature-Based Classifiers for Multispectral Remote-Sensing Images

Saroj K. Meher, B. Uma Shankar, and Ashish Ghosh

***Abstract*—The objective of this paper is to utilize the extracted features obtained by the wavelet transform (WT) rather than the original multispectral features of remote-sensing images for land-cover classification. WT provides the spatial and spectral characteristics of a pixel along with its neighbors, and hence, this can be utilized for an improved classification. Four classifiers, namely, the fuzzy product aggregation reasoning rule (FPARR), fuzzy explicit, multilayered perceptron, and neuro-fuzzy (NF), are used for this purpose. The performance is tested on multispectral real and synthetic images. The performance of original and wavelet-feature (WF)-based methods is compared. The WF-based methods have consistently yielded better results. Biorthogonal3.3 (Bior3.3) wavelet is found to be superior to other wavelets. FPARR along with the Bior3.3 wavelet outperformed all other methods. Results are evaluated using quantitative indexes like β and Xie–Beni.**

***Index Terms*—Fuzzy, land-cover classification, neural and neuro-fuzzy (NF) classification, remote sensing, wavelet transform (WT).**

I. Introduction

CLASSIFICATION of land-cover regions of remote-sensing images is essential to efficiently interpret them. This task is very complex because of low illumination quality and low spatial resolution of remotely placed sensors and rapid changes in environmental conditions. Various regions like vegetation (VEG), soil, water bodies, concrete structure, etc., are often not well separated. Thus, the gray value assigned to a pixel is an average reflectance of different types of land covers that are present in the corresponding pixel area. Therefore, a pixel may represent more than one class with varying degrees of belonging. Conventional methods cannot deal with this imprecise representation.

Fuzzy-set theory provides a useful technique to allow a pixel to be a member of more than one category [1], [2]. Attempts have been made for the remote-sensing image [3], [4] analysis using fuzzy logic [5]–[9]. A fuzzy-supervised land-cover classification method is described by Melgani *et al.* [6]. Wang and Jamshidi [7] and Shackelford and Davis [8] described the hierarchical fuzzy classification of high-resolution multispectral data of an urban area. Other applications include the estimation of subpixel component [9] and the pixel unmixing [5], etc.

Multispectral remotely sensed images comprise information over a large range of variation of frequencies, and these frequencies change over regions. These data have both spectral features with correlated bands and spatial features correlated in the same band. An efficient utilization of these spectral and spatial (contextual) information can significantly improve the classification performance. Research efforts have been made to take the advantages of local information [5], [10] for the classification of these images. These include texture features [11] extracted from angular second moments, contrast, correlation, entropy, variance, etc., which are computed from the gray level co-occurrence matrices. However, these methods are computationally expensive. Later on, Gaussian Markov random fields and Gibbs random fields were proposed to characterize textures [5]. The aforementioned conventional statistical approaches to texture analysis are restricted to the analysis of spatial interactions over the relatively small neighborhoods in a single scale.

One efficient way to deal with such problems is to recognize the input-image data by a number of subsampled approximations of it at different resolutions and desired scales, which is called multiresolution analysis [12]. In this regard, wavelet transform (WT) has received much attention as a promising tool for texture analysis in both spatial and spectral (Fourier space) domains [12]–[15] because of its ability to examine the signal at different scales that represent properties like frequency and its spatial location in the original image. Hence, the use of these coefficients (pixel with extracted features) instead of original pixel value is more justifiable. These characteristics of the WT motivated us to use it for the extraction of hidden features from remote-sensing images. Research works that are related to texture classification using WT have already been carried out [16], [17].

In this paper, we have explored the advantages of WT by incorporating it as a preprocessor for classification. In these methods, we first extract the features of the input patterns and use these features for classification. Different wavelets are used. We have considered four classifiers, namely, fuzzy product aggregation reasoning rule (FPARR) [18], fuzzy explicit (FE) [6], neural network [multilayered perceptron (MLP)] [19], and neuro-fuzzy (NF) [20]. They are tested on a synthetic image and two multispectral remote-sensing images (one four-band Indian Remote Sensing (IRS) satellite image [21] and one three-band Systeme Pour d'Observation de la Terre (SPOT) satellite image [4]) for land-cover classification. Comparison of results showed that among the proposed wavelet-feature (WF)-based classification schemes, the FPARR yielded superior results compared to others with all wavelets. The performance of the FPARR is further increased with the Biorthogonal3.3 (Bior3.3) wavelet.

Organization of this paper is as follows. Section II describes the WT-based feature extraction method. A brief description of four classifiers has been made in Section III. Results with

Manuscript received November 22, 2005; revised November 10, 2006.

The authors are with the Machine Intelligence Unit, Indian Statistical Institute, Kolkata 700108, India (e-mail: ash@isical.ac.in).

discussion have been included in Section IV. Finally, concluding remarks are made in Section V.

II. WT-Based Feature Extraction

To deal with the nonstationary behavior of signals, many research works have been carried out. Efforts are made to overcome the disadvantages of Fourier transform [12], [13] that assumes the signal to be stationary within its total range of analysis using short-time Fourier transform and WT [13], [22]. WT extends the single-scale analysis to multiscale analysis that decomposes the signal in multiple scales, where each scale represents a particular coarseness of the analyzed signal. WT tries to identify both the scale and space information of the event simultaneously which make it more useful for analysis of remote-sensing images. Further, various distinguishable characteristics like spatio-geometric information, energy at different scales, etc., which are normally called the signature of a particular land cover in remote-sensing images, are preserved in the WT-based decomposition performed with orthogonal basis [12], [22].

We have used the wavelets from different (Daubechies, Biorthogonal, Coiflets, and Symlets) groups [22]. Results are given for four wavelets as their performances are (empirically) better than others. These are Daubechies 3 (Db3), Daubechies 6 (Db6), Bior3.3, and Biorthogonal3.5 (Bior3.5) wavelets [22]. These wavelets are implemented with the multiresolution scheme given by Mallat [12], which is briefly described next for 2-D case.

A. Discrete WT and Multiresolution Analysis

The 2-D WT is performed by consecutively applying the 1-D WT on rows and columns of a 2-D image that decomposes an image into four subimages. This decomposition can be extended to more than one level providing more detailed information. To have an objective evaluation, we computed the average entropy, which provides a measure of information, of the image for each level. We found that the average-entropy value is not changing significantly after a certain level of decomposition, and we decided to decompose up to that level. For the present experiments, we stopped decomposing after the second level only. From the WT coefficients, the corresponding reconstructed images are obtained using the inverse WT, which represent the extracted features of the original image.

B. Feature Extraction

The aim of extraction of features using WT from the original spectral bands is to exploit the spatial and frequency information of the pixels. In this process, we decompose the original image into subimages (wavelet coefficients). For each level of decomposition, four subimages are obtained from each band of input image. As a whole, 16 subimages are obtained from a four-band image (original input) after one level of decomposition. It becomes 28-band subimages with two levels of decomposition and so on. These subimages are then used to reconstruct (using inverse WT) the images providing spatial and frequency information of the original image. The size of these reconstructed images is equal to the size of the original image, and there is a pixel-by-pixel correspondence between these images and the original image. The pixels in these reconstructed images, thus, maintain the functional relationship of class labels, as maintained by the original pixels. Hence, we have used these pixel values of the reconstructed images as WFs for classification. These WFs are then cascaded to get the extracted features of the original multispectral image.

III. Classification Techniques

The four classification methods used are briefed next.

A. FPARR

The FPARR classification method uses three steps [18]. In the first step, it takes the input feature vector and fuzzifies it using a π-type membership function (MF) [2]. The membership matrix $f_{d,c}(x_d)$, thus generated, expresses the degree of belonging of features to classes, where x_d is the dth feature of pattern $\mathbf{x}$ with $d = 1, 2, \ldots, D$ and $c = 1, 2, \ldots, C$.

The π-type MF can be estimated with center at $r = \text{mean}(y)$, where y is a feature of the training data. The two crossover points (let p and q) are estimated as $p = \text{mean}(y) - [\max(y) - \min(y)]/2$ and $q = \text{mean}(y) + [\max(y) - \min(y)]/2$. The membership value at the crossover point is 0.5, and at the center r, its value is maximum (i.e., 1). In the second step, the fuzzified feature values are aggregated using PRODUCT reasoning rule (PARR). It is applied on each column of the membership matrix to get the combined membership grade of features of a pattern to various classes. A hard classification output can be obtained in the last step by a defuzzification process. A MAXIMUM (MAX) operation may be used for it, and the pattern is classified to class c with the highest class membership value.

B. FE

The FE classification method [6] also uses three steps. The method uses Gaussian MF for fuzzification, minimum RR in reasoning, and MAX operation for defuzzification.

C. Neural Networks (MLP)

Here, the WFs are used as input to a feed-forward MLP network, which acts as a classifier. MLP uses back-propagation (BP) learning [19] for weight updating. The BP algorithm reduces the sum of squared error or cost function (CF) between the actual and desired output of output-layer neurons in a gradient descent manner to correct the weights. The process is continued iteratively until a target CF is achieved. The number of nodes in the input layer is equal to the number of original features or wavelet-generated features. The number of nodes in the output layer is equal to the number of classes present in the data set. Nodes in the hidden layer are equal to the square root of the product of the number of input- and output-layer nodes [19]. The weight-updating process is stopped when the corresponding CF reaches a desired value (here, it is 0.001). The

values of the parameters that have been selected empirically to get the best results are the following: momentum $= 0.83$ and learning rate $= 0.05$.

D. NF

Fuzzy and neural techniques have certain advantages of their own which are combined in the hybrid NF models. Major milestones in the NF models can be found in [23]. However, in this paper, a simple NF technique is used which is similar to the one discussed in [20]. The membership values of the features of each data pattern after fuzzification (by a π-type MF [1]) are supplied as input to the neural network (NN). The basic operations of the NN in the NF process are the same as aforementioned. The values of the parameters for the NN selected empirically are the following: momentum $= 0.79$ and learning rate $= 0.01$. The weight values are initialized between -0.5 and $+0.5$. The output of the NN, thus obtained, is defuzzified using a MAX operation, and a class label for the input data pattern is assigned using the maximum output (node) value.

IV. Results and Discussion

Selection of the training samples is made according to a prior assumption of the land-cover regions. After learning the classifier with these training samples, it is used to classify the land covers of the whole image. Various multispectral remote-sensing images from IRS-1A and SPOT are used. However, we have included only two images because these bear different characteristics like spatial resolution, number of bands, and wavelengths, while they have similar land-cover classes. Also, a synthetic image is used to support our objective.

A. Performance-Measurement Indexes

For labeled data sets, Kappa [24] value is normally used for performance measurement. However, for partially labeled data sets, as in the present case, β index [25] of homogeneity and Xie–Beni (XB) index [26] of compactness and separation, as described next, can be used for performance measurement.

1) β Index: β is defined [25] as the ratio of the total variation and within-class variation. For a given image and given number of classes, the higher the homogeneity within the classes, the higher would be the β value. Mathematically, β can be represented as $\beta = [\sum_{i=1}^{C}\sum_{j=1}^{M_i}(\mathbf{x}_{ij} - \overline{\mathbf{x}})^2 / \sum_{i=1}^{C}\sum_{j=1}^{M_i}(\mathbf{x}_{ij} - \overline{\mathbf{x}}_i)^2]$, where $\overline{\mathbf{x}}$ is the mean gray value of the image pixels (pattern vector), M_i is the number of pixels in the ith $(i = 1, 2, \ldots, C)$ class, x_{ij} is the gray value of the jth pixel $(j = 1, 2, \ldots, M_i)$ in class i, and $\overline{\mathbf{x}}_i$ is the mean of the ith class.

2) XB Index: The XB index [26] provides a validity criterion based on a function that identifies the overall compactness and separation of partitions (clusters). It is mathematically expressed as the ratio of compactness (θ) and separation (ξ), i.e., XB $= [\sum_{c=1}^{C}\sum_{z=1}^{Z}\mu_{cz}^2\|V_c - \mathbf{x}_z\|^2] / [Z \min_{c\neq j}\|V_c - V_j\|^2]$, where V_c is the centroid of the cth cluster, and $\mathbf{x}_z$ is the zth pattern. μ_{cz} is the membership value of the zth pattern to the cth cluster, and Z is the total number of patterns. The smaller the XB value, the better is the partitioning.

(a) (b)

Fig. 1. Original (a) IRS-1A (band 4) and (b) SPOT (band 3) image.

B. WF-Based Classification Process

At first, a preprocessing of the input image is performed using WT, and the corresponding WFs are extracted. For fuzzy classifiers (FPARR and FE), the extracted WFs are fuzzified using an MF (π type and Gaussian) that provides a degree of belonging of each WF to all classes, and a fuzzification matrix is generated. A suitable reasoning rule is then applied on the fuzzification matrix. At the end, a defuzzification is performed to obtain the hard class label for the input pixels. For the neural classifier, the WFs are directly fed to the NN. However, with the NF classifier, the extracted WFs are fuzzified with an MF (π type [1]), and the fuzzified values are fed to the NN. The class label for the input pixel is obtained using the defuzzification operation performed on the NN output. Classification accuracies of the WF-based classifiers are provided in tabular form, whereas the classified images with the Bior3.3 wavelet and FPARR are shown in the figures.

C. Description of Images

1) IRS-1A Image: The IRS-1A image is obtained from the Indian Remote Sensing Satellite [21]. We have used the image taken from the Linear Imaging Self-Scanner with a spatial resolution of 36.25×36.25 m and wavelength range of 0.45–0.86 μm. The whole spectrum range is decomposed into four spectral bands, namely, blue, green, red, and near infrared corresponding to bands 1, 2, 3, and 4, respectively. Since the image is poorly illuminated, we have presented the enhanced image (band 4) in Fig. 1. However, the algorithms are implemented on original image. The image covers an area around the city of Calcutta having six major land-cover classes: pure water (PW), turbid water (TW), concrete area (CON), habitation (HAB), vegetation (VEG), and open spaces (OS).

2) Synthetic Image: A four-band synthetic image (size 512×512) has been generated with six major land-cover classes similar to the IRS-1A image. Fig. 2(a) shows the synthesized image in the near-infrared range (band 4). Methods are tested on the corrupted image (with Gaussian noise having zero mean and $\sigma = 1, 2, \ldots, 6$) in all four bands. Fig. 2(b) shows the noisy version of the original image with $\sigma = 2$.

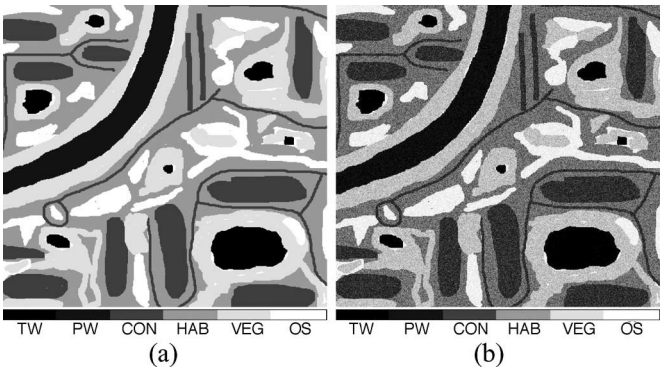

Fig. 2. Synthetic image (band 4) with (a) original and (b) noisy ($\sigma = 2$).

TABLE I
CLASSIFICATION ACCURACY (PERCENT) FOR SYNTHETIC IMAGE ($\sigma = 2$)

Classifi. method	Original features	Wavelet features			
		Bior3.3	Db3	Db6	Bior3.5
FPARR	91.23	93.35	92.91	91.57	91.78
FE	89.21	92.31	92.12	91.31	91.24
MLP	88.95	92.03	91.88	91.12	91.20
NF	90.03	92.53	92.11	91.09	91.13

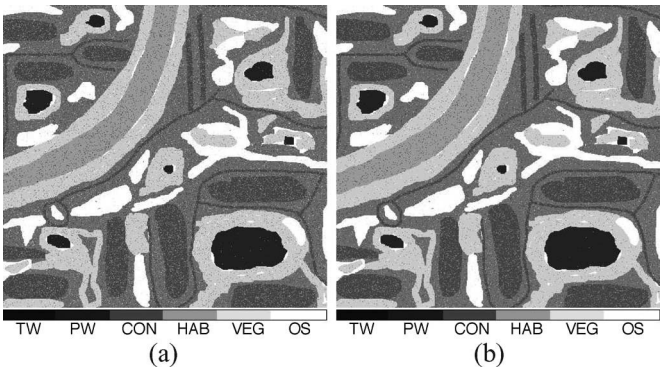

Fig. 3. Classified synthetic image by (a) FPARR and (b) Bior3.3 + FPARR.

3) SPOT Image: The SPOT image shown in Fig. 1(b) is obtained from SPOT satellite [4]. The Calcutta image has the wavelength range of 0.50–0.89 μm in three bands (green, red, and near infrared). This image has a higher spatial resolution of 20 $\times$ 20 m. We have considered the same six classes.

D. Classification of Images

1) Synthetic Image: A noisy version of the synthetic image [Fig. 2(b)] is used to test the effectiveness of the classifiers. The WFs are extracted from the four bands of noisy synthetic image and used for the land-cover classification, and the results are compared with those of the original-feature-based ones (Table I). This table showed that among the four classifiers, FPARR is providing better accuracy. Particularly, the improvement is more with Bior3.3 wavelet. This is also true for all the classifiers. For $\sigma = 2$, the classified images using FPARR classifier with original and wavelet (Bior3.3) features are shown in Fig. 3. The performance with different σ values for FPARR classifier is shown in Table II. It is observed from this table that, with the increase of noise level, the difference in percentage of classification accuracies obtained using original and WFs increases.

TABLE II
CLASSIFICATION ACCURACY (PERCENT) FOR SYNTHETIC IMAGE [DIFFERENT (σ)]

Classifi. method	σ	Original features (A)	Wavelet(Bior3.3) features (B)	Difference in accuracy (B-A)
FPARR	1	99.24	99.64	0.40
	2	91.23	93.35	2.12
	3	78.76	81.85	3.09
	4	64.45	69.32	4.87
	5	54.50	60.76	6.26
	6	47.27	55.89	8.62

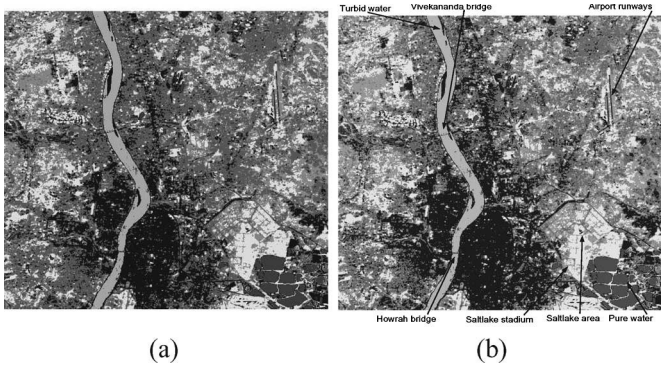

Fig. 4. Classified IRS-1A image by (a) FPARR and (b) Bior3.3 + FPARR.

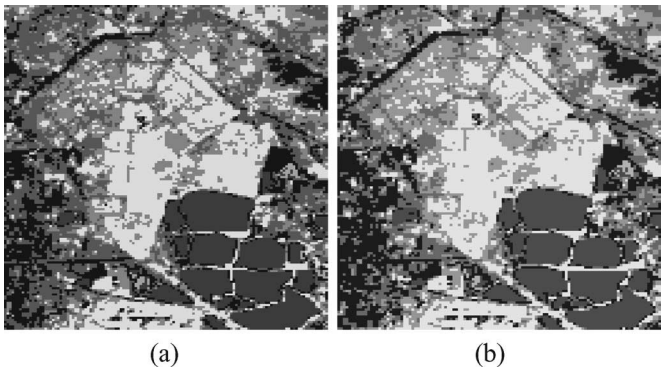

Fig. 5. (Zoomed) Some selected regions of classified IRS-1A Calcutta image with (a) FPARR and (b) WF (Bior3.3) + FPARR.

2) IRS-1A Calcutta Image: From the visualization point of view, it is observed that FPARR classification method is performing better in classifying the land covers (i.e., segregating different areas) compared to the rest three. Hence, we have shown only the FPARR classified image in Fig. 4(a). Further, the performance of all the classifiers is improved with WF; also, it is found that Bior3.3 wavelet is the best for the current problem. Thus, we have shown the classified image using the FPARR classifier with Bior3.3 wavelet in Fig. 4(b). Here, various objects like Airport runways, Saltlake Area, Saltlake Stadium, Vivekananda Bridge, Howrah Bridge, and different land-cover classes are clearly visible. These objects are more or less visible in case of other classifiers and with different WF. Thus, a zoomed version of some classified regions like Saltlake Stadium and PW is shown in Fig. 5 to get an improved visualization. From the zoomed image, it is observed that regions are more clear and distinct with the proposed method

TABLE III
β VALUES FOR DIFFERENT WF-BASED CLASSIFICATION METHODS

Classification method	wavelets	IRS Cal	SPOT Cal
Training patterns	-	9.4212	9.3343
FPARR	-	**8.1717**	**8.1078**
FE	-	7.1312	7.0137
MLP	-	7.1487	7.0341
NF	-	7.5535	7.5978
WT with FPARR	Db3	8.6348	8.7315
WT with FPARR	Db6	8.1913	8.1101
WT with FPARR	Bior3.3	**8.7413**	**8.7411**
WT with FPARR	Bior3.5	8.2012	8.1210
WT with FE	Db3	7.7017	7.6513
WT with FE	Db6	7.1934	7.1345
WT with FE	Bior3.3	**7.7918**	**7.7022**
WT with FE	Bior3.5	7.1997	7.2123
WT with MLP	Db3	7.7124	7.6121
WT with MLP	Db6	7.1935	7.2010
WT with MLP	Bior3.3	**7.7586**	**7.7143**
WT with MLP	Bior3.5	7.1678	7.2013
WT with NF	Db3	8.0112	7.9135
WT with NF	Db6	7.5963	7.6813
WT with NF	Bior3.3	**8.2138**	**8.1457**
WT with NF	Bior3.5	7.6813	7.6116

TABLE IV
XB VALUES FOR DIFFERENT WF-BASED CLASSIFICATION METHODS

Classification method	IRS Cal	SPOT Cal
FPARR	0.8310	2.1021
FE	0.9012	2.3031
MLP	0.9113	2.3200
NF	0.9001	2.2802
FPARR+Bior3.3 wavelet	**0.7672**	**1.9576**
FE+Bior3.3 wavelet	0.8687	2.1166
MLP+Bior3.3 wavelet	0.8761	2.1321
NF+Bior3.3 wavelet	0.8587	2.1001

compared to the original FPARR. With the use of WF, the classes became more separated.

Further, a concrete distinction between the various classes that are obtained by different classifiers is also justified with the quantitative index. Two quantitative indexes, namely, β and XB, have been used to justify these findings. Table III shows the results of β. As expected, the β value is the highest for the training data (9.4212) for the IRS-1A Calcutta image. Its values are 8.1717 and 7.1312 for the two fuzzy classifiers (FPARR and FE). With MLP, the β value is 7.1487, which is much closer to the value obtained with FE. With NF classifier, the β value obtained is 7.5535 which is more than that of the other classifiers except FPARR. From these β values, it is clear that the FPARR is a better classifier.

The β value is increased from 8.1717 to 8.6348, 8.1913, 8.7413, and 8.2012 for the WF-based FPARR classifier with Db3, Db6, Bior3.3, and Bior3.5 wavelets, respectively. These increments are also there for other classifiers with these wavelets. From Table III, it is clear that the FPARR classification with Bior3.3 wavelet is providing the highest β value. Similar to β index, XB index also supported the superiority of the proposed approaches. Values for XB index are shown in Table IV. It is shown that better compaction and separation of different regions of the images are obtained with the FPARR classification method compared to FE, MLP, and NF. The XB

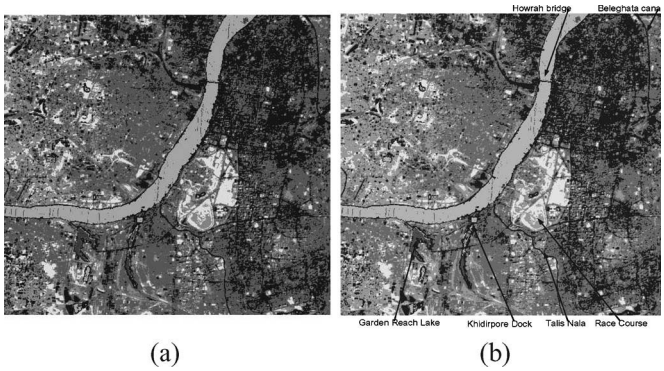

Fig. 6. Classified SPOT image by (a) FPARR and (b) Bior3.3 + FPARR.

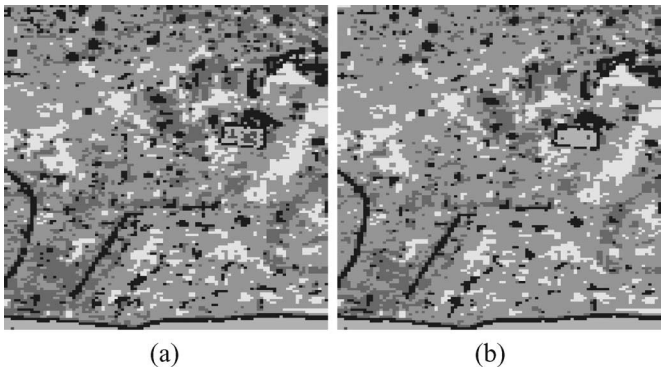

Fig. 7. (Zoomed) One selected region of classified SPOT Calcutta image with (a) FPARR and (b) WT (Bior3.3) + FPARR.

value for FPARR for IRS-1A Calcutta image is 0.8310, and is 0.9012, 0.9113, and 0.9001 for FE, MLP, and NF, respectively. Again, these values are still better for the Bior3.3 wavelet. Considering all cases, we can infer that the combination of the FPARR and Bior3.3 wavelet is outperforming the others.

3) SPOT Calcutta Image: For SPOT Calcutta image, the classified regions are shown in Fig. 6(a) for FPARR (original spectral features only) and Fig. 6(b) for the FPARR with Bior3.3 wavelet. From the figures, it is observed that all the classes are separated along with some known regions like Race Course, Howrah Bridge, Talis Nala (Canal), Beleghata Canal, Khiderpore Dock, and Garden Reach Lake. A zoomed version of a region is shown in Fig. 7 to see the differences in the classified regions more clearly. From this figure, it is evident that the proposed method produced a well-structured and proper-shaped regions compared to FPARR. However, a better performance comparison with the help of β value is shown in Table III. In a similar experiment with MLP and NF classifiers, it is observed that the WF-based methods are providing a higher β value (Table III) compared to its corresponding original spectral feature-based version. A further improvement of these classifiers with WF is observed with Bior3.3 wavelet. Like the β index, the XB values (Table IV) also corroborate the earlier findings.

V. CONCLUSION

This paper proposes a WF-based fuzzy, neural, and NF approach for classification of multispectral remote-sensing

images. The proposed method explores the possible advantages of using WT to extract features from images.

The improvement in performance of the classification scheme is verified using one synthetic image and two remote-sensing images. Various performance measures that are used to evaluate the classification results indicate that the addition of WF improves the classification accuracy. More specifically, the FPARR-based classification method with the Bior3.3 wavelet outperforms the others. Visual inspection shows that the classified regions using the proposed methods are more crisp, homogeneous, and compact compared to those obtained by the corresponding method with original features. Thus, in conclusion, we can say that, for the present set of images, the Bior3.3-based FPARR method is the best.

ACKNOWLEDGMENT

The authors would like to thank the reviewers for their valuable suggestions and the Department of Science and Technology, Government of India, for sponsoring the project "Advanced Techniques for Remote Sensing Image Processing."

REFERENCES

[1] G. J. Klir and B. Yuan, *Fuzzy Sets and Fuzzy Logic: Theory and Application*, 1st ed. Englewood Cliffs, NJ: Prentice-Hall, 1995.
[2] L. I. Kuncheva, *Fuzzy Classifier Design*. New York: Springer-Verlag, 2000.
[3] D. A. Landgrebe, *Signal Theory Methods in Multispectral Remote Sensing*. New York: Wiley, 2003.
[4] J. A. Richards and X. Jia, *Remote Sensing Digital Image Analysis: An Introduction*, 4th ed. New York: Springer-Verlag, 2006.
[5] B. Tso and P. M. Mather, *Classification Methods for Remotely Sensed Data*. New York: Taylor & Francis, 2001.
[6] F. Melgani, B. A. R. Al Hashemy, and S. M. R. Taha, "An explicit fuzzy supervised classification method for multispectral remote sensing images," *IEEE Trans. Geosci. Remote Sens.*, vol. 38, no. 1, pp. 287–295, Jan. 2000.
[7] Y. Wang and M. Jamshidi, "Fuzzy logic applied in remote sensing image classification," in *Proc. IEEE Int. Conf. Syst., Man Cybern.*, The Hague, The Netherlands, 2004, pp. 6378–6382.
[8] A. K. Shackelford and C. H. Davis, "A hierarchical fuzzy classification approach for high-resolution multispectral data over urban areas," *IEEE Trans. Geosci. Remote Sens.*, vol. 41, no. 9, pp. 1920–1932, Sep. 2003.
[9] F. Maselli, A. Rodolf, and C. Conese, "Fuzzy classification of spatially degraded thematic mapper for the estimation of sub-pixel components," *Int. J. Remote Sens.*, vol. 17, no. 3, pp. 637–651, 1996.
[10] U. Kandaswamy, D. A. Adjeroh, and M. C. Lee, "Efficient texture analysis of SAR imagery," *IEEE Trans. Geosci. Remote Sens.*, vol. 43, no. 9, pp. 2075–2083, Sep. 2005.
[11] R. M. Haralick and K. S. Shanmugam, "Combined spectral and spatial processing of ERTS imagery data," *Remote Sens. Environ.*, vol. 3, no. 1, pp. 3–13, 1974.
[12] S. Mallat, *A Wavelet Tour of Signal Processing*, 2nd ed. New York: Academic, 1999.
[13] G. Strang and T. Nguyen, *Wavelets and Filter Banks*. Cambridge, MA: Wellesley-Cambridge, 1996.
[14] L. Zhang, X. Huang, B. Huang, and P. Li, "A pixel shape index coupled with spectral information for classification of high spatial resolution remotely sensed imagery," *IEEE Trans. Geosci. Remote Sens.*, vol. 44, no. 10, pp. 2950–2961, Oct. 2006.
[15] S. Zhang, X. Xue, and X. Zhang, "Feature extraction and classification with wavelet transform and support vector machines," in *Proc. IEEE Int. Symp. Geosci. and Remote Sens.*, 2005, vol. 6, pp. 3795–3798.
[16] M. Unser, "Texture classification and segmentation using wavelet frames," *IEEE Trans. Image Process.*, vol. 4, no. 11, pp. 1549–1560, Nov. 1995.
[17] S. Arivazhagan and L. Ganesan, "Texture classification using wavelet transform," *Pattern Recognit. Lett.*, vol. 24, no. 9/10, pp. 1513–1521, Jun. 2003.
[18] A. Ghosh, S. K. Meher, and B. U. Shankar, "Fuzzy supervised classification using aggregation of features," Indian Statistical Inst., Kolkata, India, Tech. Rep. MIU/TR-02/2005, 2005.
[19] S. Haykin, *Neural Networks: A Comprehensive Foundation*. Englewood Cliffs, NJ: Prentice-Hall, 1997.
[20] S. G. Lee, J. G. Han, K. H. Chi, J. Y. Suh, H. H. Lee, M. Miyazaki, and K. Akizuki, "A neuro-fuzzy classifier for land cover classification," in *Proc. IEEE Int. Conf. Fuzzy Syst.*, 1999, pp. 1063–1068.
[21] "IRS data users hand book," 1989, NRSA, Tech. Rep., document No. IRS/NRSA/NDC/HB-02/89.
[22] I. Daubechies, *Ten Lectures on Wavelets*. Philadelphia, PA: Soc. Ind. and Appl. Math., 1992.
[23] S. K. Pal and A. Ghosh, "Neuro-fuzzy computing for image processing and pattern recognition," *Int. J. Syst. Sci.*, vol. 27, no. 12, pp. 1179–1193, 1996.
[24] J. Cohen, "A coefficient of agreement for nominal scale," *Educ. Psychol. Meas.*, vol. 20, no. 1, pp. 37–46, 1960.
[25] S. K. Pal, A. Ghosh, and B. U. Shankar, "Segmentation of remotely sensed images with fuzzy thresholding, and quantitative evaluation," *Int. J. Remote Sens.*, vol. 21, no. 11, pp. 2269–2300, Jul. 2000.
[26] X. L. Xie and G. Beni, "A validity measure for fuzzy clustering," *IEEE Trans. Pattern Anal. Mach. Intell.*, vol. 13, no. 8, pp. 841–847, Aug. 1991.

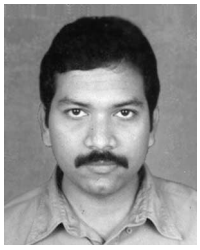

Saroj K. Meher received the Ph.D. degree in electronics engineering from the National Institute of Technology, Rourkela, India, in 2003.

He is currently a Postdoctoral Fellow in the Machine Intelligence Unit, Indian Statistical Institute, Kolkata, India. His research interest includes pattern recognition, soft computing methods, and digital signal processing. He has published many research articles in internationally reputed journals and refereed conferences.

B. Uma Shankar received the M.Sc. degree in statistics from Bhagalpur University, India, in 1985, and the Ph.D. degree in science from Jadavpur University, Kolkata, India, in 2006.

He is currently an Associate Scientist in the Machine Intelligence Unit, Indian Statistical Institute, Kolkata, India. From September 1992 to March 1993, he was at Stanford University; from June to July 1990 and June to July 1993 at CIMPA, Nice, France; and from January to March 2007 at the University of Trento, Italy. His research interests include pattern recognition and machine learning, analysis of remotely sensed images, fuzzy sets, rough sets, and neural networks. He has published many research papers in international journals and refereed conferences and is acting as a Reviewer of international journals.

Ashish Ghosh received the B.E. (Electronics) degree from Jadavpur University, Kolkata, India, in 1987 and the M.Tech. (CS) and Ph.D. degrees from the Indian Statistical Institute, Kolkata, in 1989 and 1993, respectively.

He is currently a Professor in the Machine Intelligence Unit, Indian Statistical Institute, Kolkata, India. He has been selected as an Associate of the Indian Academy of Sciences, Bangalore, in 1997. He visited various universities/academic institutes and delivered lectures in different countries, including Japan, U.S., Germany, South Korea, Poland, China, Italy, and The Netherlands. His research interests include pattern recognition and machine learning, data mining, image analysis, remotely sensed image analysis, soft computing, fuzzy sets, neural networks, evolutionary computation and bioinformatics. He has already published about 100 research papers in international journals and refereed conferences, has edited six books, and is acting as a Guest Editor of various international journals.

He received the prestigious and most coveted Young Scientists Award in Engineering Sciences from the Indian National Science Academy in 1995 and in Computer Science from the Indian Science Congress Association in 1992, respectively.